JACS Au
AN OPEN ACCESS JOURNAL OF THE AMERICAN CHEMICAL SOCIETY

pubs.acs.org/jacsau

Article

Electroassisted Propane Dehydrogenation at Low Temperatures: Far beyond the Equilibrium Limitation

Jianshuo Zhang, Ruoyun Ma, Hyungwon Ham, Ken-ichi Shimizu, and Shinya Furukawa*

Cite This: *JACS Au* 2021, 1, 1688–1693

Read Online

ACCESS | Metrics & More | Article Recommendations | Supporting Information

ABSTRACT: Propylene production by propane dehydrogenation (PDH) generally requires high temperatures due to thermodynamic equilibrium limitations. This study developed a novel type of catalytic system for low-temperature PDH by combining a surface protonics methodology with intermetallic active sites. By application of an electric current, the intermetallic Pt–In/TiO_2 catalyst gave a propylene yield of 10.2% with high selectivity, even at 250 °C, where the thermodynamic equilibrium yield was only 0.15%. Electroassisted proton collisions with propane allowed an unusual reaction pathway for low-temperature PDH. Alloying of Pt with In drastically enhanced the activity and selectivity due to the increased electron density of Pt.

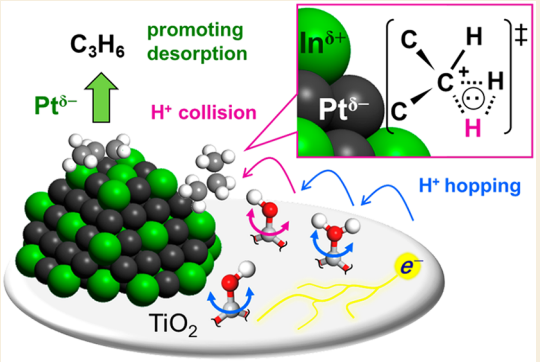

KEYWORDS: *electric field, propane dehydrogenation, intermetallic compounds, equilibrium limitation, catalysis*

INTRODUCTION

Propylene is one of the most important base chemicals in industry for the production of polymers, resins, solvents, and other fine chemicals.[1−3] The global propylene demand has been increasing due to the recent shift in feedstock from oil-based naphtha to shale-based ethane and the corresponding increase in ethane crackers.[1−3] Catalytic propane dehydrogenation (PDH) is a promising way to fill the "propylene gap". It has been a topical theme in pure and applied chemistry; the increased numbers of papers and reviews on this topic illustrate this.[1−3] Due to its endothermicity, PDH requires temperatures of higher than 600 °C to obtain sufficiently high propane conversion. However, undesirable side reactions, such as overdehydrogenation, C–C cracking, and coking, typically occur at such high temperatures, resulting in catalyst deactivation after a short period due to coke accumulation.[1−3] The recent research trend has been to design a catalyst with long-term stability, even at high temperatures.[1−3] On the other hand, such high-temperature processes are highly energy consuming and require a high cost for operation.

Another possible and pioneering approach is the development of a novel catalytic system that can produce propylene at low temperatures. Using an external-force system, such as photoassisted, electroassisted, or plasma-assisted catalysis, the low equilibrium conversion of propane can be boosted due to the large gain in free energy. Electroassisted catalysis using "surface protonics" is a promising methodology for such a low-temperature conversion.[4,5] By imposition of an electric field to a catalyst, proton hopping via surface hydroxyl groups known as the Grotthuss mechanism can be facilitated,[4,5] enabling strong proton collisions with reactant molecules. Robust molecules, such as N_2,[6] CH_4,[7] and CO_2,[8,9] can be activated by surface protonics and transformed to value-added chemicals, even at low temperatures (NH_3, H_2, or CO at 150–300 °C). Although this methodology is also valid for low-temperature PDH, there is another problem; the propylene product is more reactive than the reactant propane. Therefore, the undesirable decomposition of propylene can be triggered by strong proton collisions. Hence, retaining high propylene selectivity is a challenge in electroassisted PDH in comparison to conventional thermal PDH.

This paper reports that a combination of a surface protonics methodology with intermetallic active sites could overcome this challenge. The alloying of Pt with In significantly improved the propylene selectivity and greatly enhanced the catalytic activity. In this process, a 2 orders of magnitude higher propylene yield (10.2%) in comparison to that at thermodynamic equilibrium (0.1% at 250 °C) was achieved. This paper reports this novel and efficient catalytic system for PDH that works efficiently at low temperatures.

Received: June 24, 2021
Published: August 31, 2021

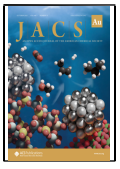

https://doi.org/10.1021/jacsau.1c00287
JACS Au 2021, 1, 1688–1693

RESULTS AND DISCUSSION

The catalysts were prepared by a conventional impregnation method using TiO_2 as a catalyst support capable of surface protonics (Pt/TiO_2 and $Pt–In/TiO_2$: Pt 3 wt %). Figure 1

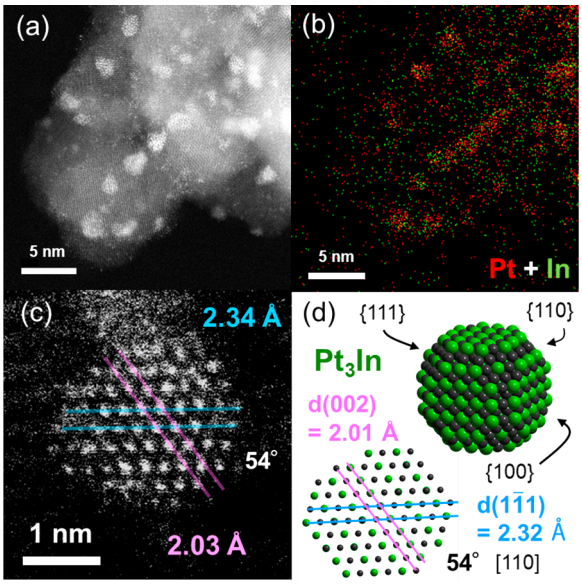

Figure 1. (a) HAADF-STEM image of $Pt–In/TiO_2$ and (b) the corresponding elemental map acquired by EDX. (c) High-resolution HAADF-STEM image of a single nanoparticle. (d) Model structure of intermetallic Pt_3In viewed along the [110] direction.

shows the high-angle annular dark-field scanning transmission electron microscopy (HAADF-STEM) image of $Pt–In/TiO_2$ and the corresponding elemental map of Pt and In (Figure S1 for Ti and O). Small 1–2 nm diameter nanoparticles consisting of Pt and In were highly dispersed over the TiO_2 surface. Quantitative analysis of some Pt–In bimetallic nanoparticles showed a Pt/In atomic ratio of approximately 3 (Figure S2). The high-resolution image revealed a specific atomic arrangement with interplanar distances of 2.03 and 2.34 Å and a dihedral angle of 54°, which agreed well with those of intermetallic Pt_3In viewed along the [110] direction.[10] The formation of intermetallic Pt_3In was also indicated by an extended X-ray absorption fine structure analysis (XAFS), where Pt–In (In–Pt) scattering was observed in both Pt L_{III} and In K edges (Figures S3–S5 and Table S1).

The XAFS analysis also provided additional information on the electronic state of Pt. As can be observed in the Pt L_{III} X-ray absorption near-edge structure (Figure 2), the white-line intensity decreased after alloying with In. This suggests that the occupation of the d orbital (electron density of Pt) was increased by In, which is consistent with the trend reported elsewhere.[11]

CO pulse chemisorption showed that the Pt dispersion of $Pt–In/TiO_2$ was 22.7%, which is consistent with that predicted from a cuboctahedral model of a 2–3 nm Pt_3In nanoparticle (23.2%; Figure S6).

The prepared catalysts were tested in PDH using a fixed-bed continuous flow reactor. Two stainless steel rods as electrodes were placed in contact with the top and bottom of the catalyst bed to impose a direct current to the catalyst (Figure 3a; see also Figure S7 for details). Before the reaction, the catalyst was pretreated with flowing H_2 at 300 °C, so that the metal

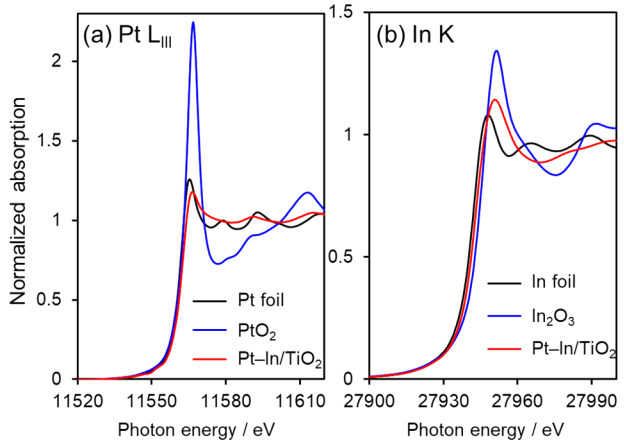

Figure 2. (a) Pt L_{III} and (b) In K edge XANES spectra of $Pt–In/TiO_2$ and reference compounds.

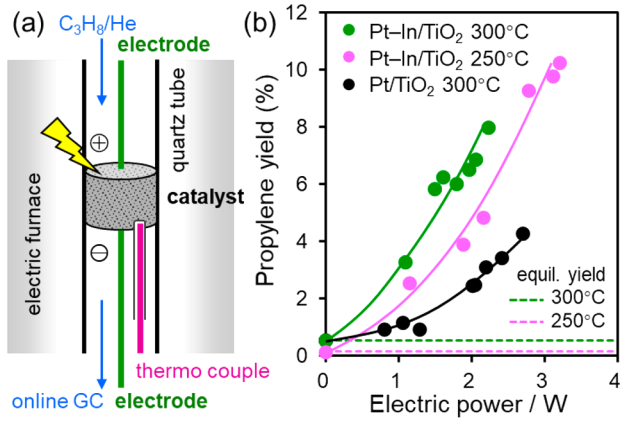

Figure 3. (a) Illustration of the reactor setup for electroassisted PDH. (b) Dependence of propylene yield on the electric power supplied to the catalytic system. The furnace temperature was set to 250 or 300 °C.

nanoparticles and TiO_2 were reduced. Partial reduction of the TiO_2 support is necessary to pass an electric current to the catalyst bed. Figure 3b represents the dependence of the propylene yield on the electric power supplied to the system.

The propylene yield was virtually zero when no electricity was supplied due to thermodynamic limitations (0.15% and 0.55% at 250 and 300 °C, respectively; Figure S8). The propylene yields increased monotonously with an increase in the supplied electric power, showing a significant dependence on the electric power (carbon balances were mostly 0.95–1.00; Figure S9). Interestingly, $Pt–In/TiO_2$ exhibited a remarkably higher propylene yield in comparison to Pt/TiO_2 (ca. 3 times the higher yield per watt, at 300 °C). The reaction still proceeded even at 250 °C (the voltage and current are shown in Figure S10), where the highest propylene yield of 10.2% was achieved using 3.2 W of electric power. The catalyst bed temperature did not increase significantly during energization (typically +2 to +5 °C at a furnace temperature of 250 °C; Figure S11), indicating that Joule heating made a negligible contribution to catalysis. Thus, a 2 orders of magnitude higher propylene yield in comparison to the thermodynamic equilibrium limitation (0.15%) was achieved. To the best of our knowledge, propylene has been obtained successfully via PDH in this temperature region for the first time. Moreover, the propylene selectivity was improved: although Pt/TiO_2

https://doi.org/10.1021/jacsau.1c00287
JACS Au 2021, 1, 1688–1693

showed low selectivity due to the formation of C1 and C2 byproducts (59−79%), Pt−In/TiO_2 gave good selectivity (typically, 84−99%; Figure S12). Thus, both the activity and the selectivity were drastically enhanced by alloying Pt with In, affording an efficient catalyst for low-temperature PDH. In addition, no catalyst deactivation was observed after 120 min of electroassisted PDH (Figure S13).

Next, kinetic studies were performed to understand the reaction mechanism of electroassisted PDH on Pt−In/TiO_2. The dependences of the reaction rate on the partial pressure of propane ($P_{C_3H_8}$) and electric power (E_p) at 300 °C were 0.75 and 1.21, respectively (Figure S14). The dependence on E_p increased to 1.44 at 250 °C. The reaction order for E_p was higher than unity, suggesting that more than one elementary step is promoted by electricity. Figure 4 shows the Eyring plots of thermally assisted and electroassisted PDH using Pt−In/TiO_2.

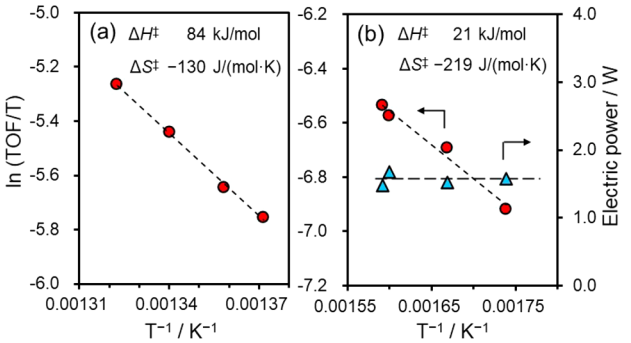

Figure 4. Eyring plots for (a) thermal and (b) electroassisted PDH over Pt−In/TiO_2.

In the absence of electricity, the obtained $\Delta H^{\ddagger}$ and $\Delta S^{\ddagger}$ values were similar to those obtained in thermal PDH using Pt-based catalysts.[12,13] On the other hand, the $\Delta H^{\ddagger}$ and $\Delta S^{\ddagger}$ values both decreased drastically when a current was applied. Here, the electric power was adjusted to be almost constant at each temperature to exclude its effects on the reaction rate. The significant decrease in the $\Delta S^{\ddagger}$ value suggests that the rate-determining step (RDS) had changed to a less entropic pathway. When it is considered that proton hopping is a crucial step of surface protonics, changing from C−H scission of propane (dissociative, generally the RDS of PDH) to proton collision on propane (associative) is most likely. The quite low $\Delta H^{\ddagger}$ value (21 kJ mol^{-1}) indicates that the proton-hopping/collision process is electrically biased by the external electric field (Figure S15). Similar low values of apparent activation energies were also reported in electrochemistry[14,15] and other electroassisted catalyses.[16−18] Thus, electroassisted PDH provides a novel reaction pathway with a much lower activation barrier. The electrically biased proton also provides a free energy gain to the initial state of the PDH, which decreases the overall ΔG value and increases the equilibrium propane conversion (Figure S15). The kinetic isotope effect (KIE) was examined next to obtain further information on the reaction mechanism. For thermal PDH, a normal KIE (k_H/k_D = 1.95) was observed when fully deuterated propane (C_3D_8) was used as the reactant, demonstrating that the C−H scission of propane is the RDS. Surprisingly, inverse KIE values were reproducibly obtained when a current was applied (k_H/k_D = 0.69−0.81; Table S2), indicating that C−H scission is not the RDS. A possible interpretation of the inverse KIE is the involvement of a nonlinear three-center transition state, in which new bond formation occurs simultaneously with the old bond scission.[19] This is because a three-center transition state has a larger coupling constant of vibration in comparison to the initial physisorbed state;[20,21] therefore, the zero-point energy (ZPE) difference between H and D species becomes larger (Figure 5) at the transition state than at the initial state. Here,

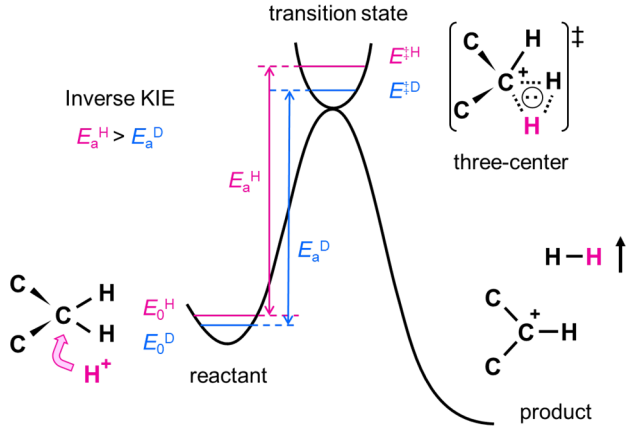

Figure 5. Possible interpretation for the potential energy profiles yielding inverse KIE.

the ZPE values at the initial and transition states are described by eqs 1 and 2, respectively[21]

$$E_0^{H(D)} = \frac{h}{4\pi}\sqrt{\frac{k_0}{\mu_{H(D)}}} \quad (1)$$

$$E^{\ddagger H(D)} = \frac{h}{4\pi}\sqrt{\frac{k^{\ddagger}}{\mu_{H(D)}}} \quad (2)$$

where, h, k, and μ indicate the Planck constant, the coupling constant of vibration, and the reduced mass, respectively. The ZPE difference between H and D species for the initial and transition states can be expressed by eqs 3 and 4, respectively:

$$\Delta E_0^{H-D} = E_0^H - E_0^D = \frac{h}{4\pi}\left(\sqrt{\frac{1}{\mu_H}} - \sqrt{\frac{1}{\mu_D}}\right)\sqrt{k_0} \quad (3)$$

$$\Delta E^{\ddagger H-D} = E^{\ddagger H} - E^{\ddagger D} = \frac{h}{4\pi}\left(\sqrt{\frac{1}{\mu_H}} - \sqrt{\frac{1}{\mu_D}}\right)\sqrt{k^{\ddagger}} \quad (4)$$

On consideration that the coupling constant of vibration of a three-center transition state is larger than that of the initial physisorbed state, the following relationship is obtained (eq 5):

$$\Delta E^{\ddagger H-D} > \Delta E_0^{H-D} \quad \sqrt{k^{\ddagger}} > \sqrt{k_0} \quad (5)$$

Therefore, the energy barrier of D collision should be lower than that of H collision as follows (eq 6):

$$E_a^H - E_a^D = E^{\ddagger H} - E_0^H - (E^{\ddagger D} - E_0^D) = \Delta E^{\ddagger H-D} - \Delta E_0^{H-D} > 0 \quad (6)$$

Thus, the three-center transition state mechanism can explain the inverse KIE and is consistent with the proton collision pathway. Indeed, a previous study on quantum chemical

https://doi.org/10.1021/jacsau.1c00287
JACS Au 2021, 1, 1688−1693

analysis for H^+ attack on C_3H_8 reported inverse KIE values.[22] On the basis of these results, it is believed that proton collision on propane that involves a three-center transition state is the RDS of the electroassisted PDH over Pt−In/TiO_2.

A kinetic analysis was also conducted using the experimental reaction orders and the following reaction scheme of the electroassisted PDH

$$H^+\cdot\sigma_0 \rightleftharpoons H^+\cdot\sigma_i \tag{7}$$

$$C_3H_8 + \sigma_m \rightleftharpoons C_3H_8\cdot\sigma_m \tag{8}$$

$$C_3H_8\cdot\sigma_m + H^+\cdot\sigma_i \rightarrow C_3H_7^+\cdot\sigma_m + H_2 + \sigma_i \tag{9}$$

$$C_3H_7^+\cdot\sigma_m + \sigma_i \rightleftharpoons C_3H_6\cdot\sigma_m + H^+\cdot\sigma_i \tag{10}$$

$$C_3H_6\cdot\sigma_m \rightleftharpoons C_3H_6 + \sigma_m \tag{11}$$

where σ_0, σ_i, and σ_m indicate a proton acceptor on the surface (excess), a proton acceptor at the metal−support interface, and a metallic adsorption site, respectively. These equations represent the following: (eq 7) proton hopping, (eq 8) propane physisorption, (eq 9) proton collision to propane, (eq 10) propylene formation (deprotonation), and (eq 11) propylene desorption. In eq 9, a three-center transition state, such as C···H_2, is assumed (Figure 5). Here, eqs 7, 9, and 10 could be facilitated by an electric field because cationic species are involved. We solved the rate equation of eq 9 as the RDS by applying a quasi-stationary approximation and site conservation condition as follows (see Note 1 in the Supporting Information for details)

$$r = \frac{k_3K_1K_2C_0P_{C_3H_8}E_p}{1 + K_2P_{C_3H_8} + K_5^{-1}P_{C_3H_6} + \frac{K_4^{-1}K_5^{-1}P_{C_3H_6}}{(K_1^{-1}C_0^{-1} - 1)E_p}} \tag{12}$$

where k_i, K_i, and C_0 are the rate and equilibrium constants of step i and the surface proton density, respectively. This rate equation can be simplified into the following form using some approximations

$$r = kP_{C_3H_8}{}^{\alpha}E_p{}^{\beta} \tag{13}$$

where, the lower/higher limits of α and β are 0/1 and 1/2, respectively (see Note 1 in the Supporting Information for the derivation). Thus, the possible reaction order ranges can be obtained as

$$\therefore 0 < \alpha < 1,\ 1 < \beta < 2 \tag{14}$$

which are fully consistent with the experimental orders (α = 0.75 and β = 1.21 or 1.44). The good agreement between the theoretical and experimental reaction orders supports the validity of the proposed reaction mechanism. Figure 6 presents a summary of the reaction mechanism.

Under an electric field, H^+ hopping is facilitated by the Grotthuss mechanism and H^+ collisions with propane allow its activation via a three-center transition state to generate $C_3H_7^+$ and H_2. Here, alloying of Pt with In promotes this process, probably because the electron-enriched Pt stabilizes the cationic transition state and $C_3H_7^+$ intermediate. The $C_3H_7^+$ intermediate is then converted to C_3H_6 and H^+ is recovered. The electron-enriched Pt can also enhance propylene desorption because of the weaker adsorption, which decreases the probability of propylene decomposition and increases its selectivity. Indeed, our DFT calculation revealed that the adsorption energy of C_3H_6 on Pt(111) and Pt_3In(111) were

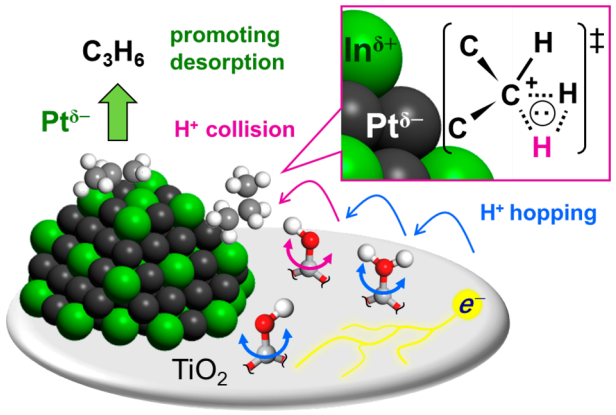

Figure 6. Proposed reaction mechanism of electroassisted PDH over Pt−In/TiO_2.

−102.0 and −58.1 kJ mol^{-1}, respectively (Figure S16), which strongly supports the enhanced desorption of propylene on Pt−In/TiO_2. In this context, the propylene selectivity might be further improved by using more In-rich intermetallic phases to promote propylene desorption. Thus, Pt−In/TiO_2 works as an efficient catalyst for electroassisted PDH at low temperatures.

Finally, the energy efficiency of this catalytic system was evaluated and compared with that of the thermal reaction. For a propylene yield of 10.2% at 250 °C, the estimated enthalpy gain from the endothermic propylene production (ΔH = +127.5 kJ mol^{-1}) was 0.090 J s^{-1} (W), which corresponds to a 2.8% energy efficiency for the supplied electric power of 3.2 W. Although there is room for improvement, this efficiency may be much greater than that in thermal reactions because a much higher temperature is needed to obtain comparable propylene yields (e.g., 460 °C for a 10.3% yield). For example, in the present case, 22 W of additional energy is required to heat the electric furnace from 250 to 460 °C (Figure S17). Although this is a specific case and the efficiency differs according to the individual experimental setup, these results suggest that the electroassisted PDH has much greater energy efficiency in comparison to the thermal reactions.

CONCLUSIONS

In summary, a novel type of catalytic system was developed for PDH by the combination of a surface protonics methodology and active site modification based on intermetallics. With the aid of 3.2 W electric power, Pt−In/TiO_2 afforded a 10.2% propylene yield at 250 °C for the first time, where the thermodynamic equilibrium yield was only 0.15%. Alloying of Pt with In drastically modified the electronic state of Pt, which enhanced both the catalytic activity and selectivity. Overall, this study opens a new horizon for the catalysis of PDH.

METHODS

Catalyst Preparation

For electroassisted catalysis, a reducible oxide support that has surface hydroxyl groups should be used because conductivity and surface protons are necessary for surface protonics. In this study, Degussa P25 TiO_2 was used as a catalyst support. The Pt/TiO_2 and Pt−In/TiO_2 catalysts were prepared by an (co)impregnation method using an excess amount of water (ca. 25 mL of ion-exchanged water per g of support). The TiO_2 support was added to a vigorously stirred aqueous solution containing $Pt(NH_3)_2(NO_3)_2$ (Furuya Metal Co. Ltd., purchased as an aqueous solution with 4.96 wt % of Pt) and/or

https://doi.org/10.1021/jacsau.1c00287
JACS Au 2021, 1, 1688−1693

$In(NO_3)_3 \cdot 8.8H_2O$ (Kanto, 99%), followed by stirring for 3 h. The mixture was dried under reduced pressure at 50 °C, followed by reduction under flowing H_2 (50 mL min^{-1}) at 500 °C for 1 h. The loading amount of Pt was adjusted to 3.0 wt %, and the Pt/In ratio was fixed to 1.

Characterization

HAADF-STEM analysis was carried out using a JEOL JEM-ARM200 M microscope equipped with an energy dispersive X-ray (EDX) analyzer (EX24221M1G5T) at an accelerating voltage of 200 kV. To prepare the TEM specimen, all samples were sonicated in ethanol and then dispersed on a Mo grid supported by an ultrathin carbon film.

CO pulse chemisorption was performed for all the prepared catalysts using a BELCAT II instrument (Microtrac BEL) to estimate the dispersion of Pt. Prior to chemisorption, the catalyst was pretreated under a 5% H_2/Ar flow (40 mL min^{-1}) at 400 °C for 0.5 h. After the reduction pretreatment, He was introduced at the same temperature for 10 min to remove the chemisorbed hydrogen, followed by cooling to room temperature. A 10% CO/He pulse was introduced into the reactor, and the supplied CO flow was quantified downstream by a thermal conductivity detector. The metal dispersion was calculated as a fraction (%) of exposed Pt to those in the catalyst, assuming a 1:1 adsorption stoichiometry.

XAFS measurements of the Pt−In/TiO_2 catalyst and reference foils were performed at the BL14B2 beamline of SPring-8, Japan Synchrotron Radiation Research Institute. A Si(111) or Si(311) double crystal was used as a monochromator. The spectra were recorded at the Pt L_{III} and In K edges in transmission modes at room temperature. First, the catalyst was pressed into a pellet (diameter 7 mm) and reduced under flowing H_2 at 500 °C for 0.5 h. Then, the reduced sample was then transferred into an Ar glovebox (O_2 <0.001 ppm) without exposure to air and sealed in a plastic bag (Barrier Nylon) with an ISO A500-HS oxygen absorber (Fe powder). The measurements for foil samples were done in air. The obtained XAFS spectra were analyzed using Athena and Artemis software ver. 0.9.25 included in the Demeter package.[23] The k^3-weighted EXAFS oscillation was Fourier-transformed in the k range of 3−12 $Å^{-1}$ for all samples. Curve fitting was performed using the back Fourier transforms of the coordination peaks in the ranges 1.5−3.0 and 1.5−3.7 $Å^{-1}$ for Pt L_{III} and In K edges, respectively. The backscattering amplitude and phase shift functions were calculated by FEFF8.[24]

Catalytic Reaction

Thermal and electroassisted PDH was carried out using a continuous flow fixed-bed quartz reactor with a 6 mm internal diameter. The detailed setup of the reactor is shown in Figure S7. The Pt/TiO_2 or Pt−In/TiO_2 catalyst (100 mg of Pt: 3 wt %, powder) was placed on a piece of glass wool in the quartz tube reactor. Two stainless steel rods (φ 2 mm) were inserted into the reactor as electrodes and contacted with the top and bottom of the catalyst bed. A K-type thermocouple covered with a glass capillary tube (for insulation protection) was also contacted with the catalyst bed to measure the catalyst bed temperature separately from the furnace temperature. Prior to the catalytic reaction, the catalyst was pretreated under flowing H_2/He (5/10 mLmin^{-1}) at 300 °C for 0.5 h, followed by purging under flowing He (10 mLmin^{-1}) at the reaction temperature. A constant direct current (5−60 mA) was imposed to the catalyst bed using a high-voltage DC power supply (Tektronix Keithley SMU 2657A). Activity tests were conducted under a reaction gas flow (C_3H_8/He = 10/10 mL min^{-1}) at specific temperatures (250−330 °C for electroassisted PDH and 450−480 °C for thermal PDH). The product gas was analyzed using a thermal conductivity detection gas chromatograph (Shimadzu GC-8A, column Unipak S). The C_3H_8 conversion, C_3H_6 selectivity, C_3H_6 yield, and carbon balance were defined as follows:

$$C_3H_8 \text{ conversion: } X_{C_3H_8}\,(\%) = \frac{[C_3H_8]_{in} - [C_3H_8]_{out}}{[C_3H_8]_{in}} \times 100$$

$$C_3H_6 \text{ selectivity: } S_{C_3H_6}\,(\%) = \frac{[C_3H_6]_{out} \times 100}{[C_3H_6]_{out} + \frac{2}{3}[C_2H_6]_{out} + \frac{2}{3}[C_2H_4]_{out} + \frac{1}{3}[CH_4]_{out}}$$

$$C_3H_6 \text{ yield: } Y_{C_3H_6}\,(\%) = \frac{X_{C_3H_8} \cdot S_{C_3H_6}}{100}$$

$$\text{Carbon balance: } C_b\,(\%) = \frac{[C_3H_8]_{out} + [C_3H_6]_{out} + \frac{2}{3}[C_2H_6]_{out} + \frac{2}{3}[C_2H_4]_{out} + \frac{1}{3}[CH_4]_{out}}{[C_3H_8]_{in}}$$

Computational Details

Periodic DFT calculations were performed using the CASTEP code[25] with Vanderbilt-type ultrasoft pseudopotentials[26] and the revised version of the Perdew−Burke−Ernzerhof exchange-correlation functional based on the generalized gradient approximation.[27] The plane-wave basis set was truncated at a kinetic energy of 360 eV, and a Fermi smearing of 0.1 eV was utilized. Dispersion correlations were considered using the Tkatchenko−Scheffler method with a scaling coefficient of s_R = 0.94 and a damping parameter of d = 20.[28] The reciprocal space was sampled using a k-point mesh with a spacing of typically 0.04 $Å^{-1}$, as generated by the Monkhorst−Pack scheme.[29] Spin polarization was considered with net-zero charge in all of the calculations. Geometry optimization was performed on supercell structures using periodic boundary conditions. The surface was modeled based on Pt(111)−(2 × 2) and Pt_3In(111)−(1 × 1) slabs that were four atomic layers thick with 13 Å of vacuum spacing. The convergence criteria for structure optimization and energy calculation were set to (a) an SCF tolerance of 1.0×10^{-6} eV per atom, (b) an energy tolerance of 1.0×10^{-5} eV per atom, (c) a maximum force tolerance of 0.05 eV $Å^{-1}$, and (d) a maximum displacement tolerance of 1.0×10^{-3} Å. The adsorption energy (E_{ad}) was defined as follows: $E_{ad} = E_{A\text{-}S} - (E_S + E_A)$, where $E_{A\text{-}S}$ is the energy of the slab together with the adsorbate, E_A is the total energy of the free adsorbate, and E_S is the total energy of the bare slab.

■ ASSOCIATED CONTENT

Supporting Information

The Supporting Information is available free of charge at https://pubs.acs.org/doi/10.1021/jacsau.1c00287.

HAADF-STEM data, XAFS data, catalytic reaction, and kinetic analysis (PDF)

■ AUTHOR INFORMATION

Corresponding Author

Shinya Furukawa − *Institute for Catalysis, Hokkaido University, Sapporo 001-0021, Japan; Elements Strategy Initiative for Catalysts and Batteries, Kyoto University, Kyoto 615-8520, Japan; Japan Science and Technology Agency, PRESTO, Tokyo 102-0076, Japan;* orcid.org/0000-0002-2621-6139; Email: furukawa@cat.hokudai.ac.jp

Authors

Jianshuo Zhang − *Institute for Catalysis, Hokkaido University, Sapporo 001-0021, Japan*

Ruoyun Ma − *Institute for Catalysis, Hokkaido University, Sapporo 001-0021, Japan*

Hyungwon Ham − *Institute for Catalysis, Hokkaido University, Sapporo 001-0021, Japan*

Ken-ichi Shimizu − *Institute for Catalysis, Hokkaido University, Sapporo 001-0021, Japan; Elements Strategy Initiative for Catalysts and Batteries, Kyoto University, Kyoto 615-8520, Japan;* orcid.org/0000-0003-0501-0294

https://doi.org/10.1021/jacsau.1c00287
JACS Au 2021, 1, 1688−1693

Complete contact information is available at:
https://pubs.acs.org/10.1021/jacsau.1c00287

Notes

The authors declare no competing financial interest.

■ ACKNOWLEDGMENTS

This work was supported by JST PRESTO (JPMJPR19T7) and JSPS KAKENHI (Grant Nos. 17H04965 and 20H02517). The XAFS analysis was performed with the approval of JASRI (No. 2020A1609). We appreciate the technical staff of the Research Institute for Electronic Science, Hokkaido University, for help with HAADF-STEM observations.

■ REFERENCES

(1) Dai, Y. H.; Gao, X.; Wang, Q. J.; Wan, X. Y.; Zhou, C. M.; Yang, Y. H. Recent progress in heterogeneous metal and metal oxide catalysts for direct dehydrogenation of ethane and propane. *Chem. Soc. Rev.* **2021**, *50*, 5590−5630.
(2) Chen, S.; Chang, X.; Sun, G. D.; Zhang, T. T.; Xu, Y. Y.; Wang, Y.; Pei, C. L.; Gong, J. L. Propane dehydrogenation: catalyst development, new chemistry, and emerging technologies. *Chem. Soc. Rev.* **2021**, *50*, 3315−3354.
(3) Sattler, J. J. H. B.; Ruiz-Martinez, J.; Santillan-Jimenez, E.; Weckhuysen, B. M. Catalytic Dehydrogenation of Light Alkanes on Metals and Metal Oxides. *Chem. Rev.* **2014**, *114*, 10613−10653.
(4) Torimoto, M.; Murakami, K.; Sekine, Y. Low-Temperature Heterogeneous Catalytic Reaction by Surface Protonics. *Bull. Chem. Soc. Jpn.* **2019**, *92*, 1785−1792.
(5) Manabe, R.; Okada, S.; Inagaki, R.; Oshima, K.; Ogo, S.; Sekine, Y. Surface Protonics Promotes Catalysis. *Sci. Rep.* **2016**, *6*, 38007.
(6) Manabe, R.; Nakatsubo, H.; Gondo, A.; Murakami, K.; Ogo, S.; Tsuneki, H.; Ikeda, M.; Ishikawa, A.; Nakai, H.; Sekine, Y. Electrocatalytic synthesis of ammonia by surface proton hopping. *Chem. Sci.* **2017**, *8*, 5434−5439.
(7) Oshima, K.; Shinagawa, T.; Sekine, Y. Methane Conversion Assisted by Plasma or Electric Field. *J. Jpn. Pet. Inst.* **2013**, *56*, 11−21.
(8) Yabe, T.; Yamada, K.; Murakami, K.; Toko, K.; Ito, K.; Higo, T.; Ogo, S.; Sekine, Y. Role of Electric Field and Surface Protonics on Low-Temperature Catalytic Dry Reforming of Methane. *ACS Sustainable Chem. Eng.* **2019**, *7*, 5690−5697.
(9) Yabe, T.; Mitarai, K.; Oshima, K.; Ogo, S.; Sekine, Y. Low-temperature dry reforming of methane to produce syngas in an electric field over La-doped Ni/ZrO_2 catalysts. *Fuel Process. Technol.* **2017**, *158*, 96−103.
(10) Lin, C. F.; Mohney, S. E.; Chang, Y. A. Phase-Equilibria in the Pt-in-P System. *J. Appl. Phys.* **1993**, *74*, 4398−4402.
(11) Zakharova, E. Y.; Andreeva, N. A.; Kazakov, S. M.; Kuznetsov, A. N. Ternary arsenides based on platinum-indium and palladium-indium fragments of the Cu_3Au-type: Crystal structures and chemical bonding. *J. Alloys Compd.* **2015**, *621*, 307−313.
(12) Zhang, W.; Wang, H. Z.; Jiang, J. W.; Sui, Z. J.; Zhu, Y. A.; Chen, D.; Zhou, X. G. Size Dependence of Pt Catalysts for Propane Dehydrogenation: from Atomically Dispersed to Nanoparticles. *ACS Catal.* **2020**, *10*, 12932−12942.
(13) Escorcia, N. J.; LiBretto, N. J.; Miller, J. T.; Li, C. W. Colloidal Synthesis of Well-Defined Bimetallic Nanoparticles for Nonoxidative Alkane Dehydrogenation. *ACS Catal.* **2020**, *10*, 9813−9823.
(14) Zhou, M.; Weng, Q.; Zhang, X.; Wang, X.; Xue, Y.; Zeng, X.; Bando, Y.; Golberg, D. In Situ Electrochemical Formation of Core-Shell Nickel-Iron Disulfide and Oxyhydroxide Heterostructured Catalysts for a Stable Oxygen Evolution Reaction and the Associated Mechanisms. *J. Mater. Chem. A* **2017**, *5*, 4335−4342.
(15) Madram, A. R.; Asadi, S. Kinetics of the hydrogen evolution reaction on a highly porous three-dimensional Ni catalyst in the presence of a Mo ion activator in alkaline solution. *New J. Chem.* **2017**, *41*, 3344−3351.
(16) Gondo, A.; Manabe, R.; Sakai, R.; Murakami, K.; Yabe, T.; Ogo, S.; Ikeda, M.; Tsuneki, H.; Sekine, Y. Ammonia Synthesis over Co Catalyst in an Electric Field. *Catal. Lett.* **2018**, *148*, 1929−1938.
(17) Takise, K.; Sato, A.; Murakami, K.; Ogo, S.; Seo, J. G.; Imagawa, K.; Kado, S.; Sekine, Y. Irreversible catalytic methylcyclohexane dehydrogenation by surface protonics at low temperature. *RSC Adv.* **2019**, *9*, 5918−5924.
(18) Takise, K.; Sato, A.; Muraguchi, K.; Ogo, S.; Sekine, Y. Steam reforming of aromatic hydrocarbon at low temperature in electric field. *Appl. Catal., A* **2019**, *573*, 56−63.
(19) Wiberg, K. B. The Deuterium Isotope Effect. *Chem. Rev.* **1955**, *55*, 713−743.
(20) Kurylo, M. J.; Linden, G. A.; Timmons, R. B. ESR Study of the Kinetic Isotope Effect in the Reaction of H and D Atoms with CH_4. *J. Chem. Phys.* **1970**, *52*, 1773−1781.
(21) Okada, S.; Manabe, R.; Inagaki, R.; Ogo, S.; Sekine, Y. Methane dissociative adsorption in catalytic steam reforming of methane over Pd/CeO_2 in an electric field. *Catal. Today* **2018**, *307*, 272−276.
(22) Kerkeni, B.; Clary, D. C. Quantum reactive scattering of H^+ hydrocarbon reactions. *Phys. Chem. Chem. Phys.* **2006**, *8*, 917−925.
(23) Ravel, B.; Newville, M. ATHENA, ARTEMIS, HEPHAESTUS: Data Analysis for X-Ray Absorption Spectroscopy Using IFEFFIT. *J. Synchrotron Radiat.* **2005**, *12*, 537−541.
(24) Ankudinov, A.; Ravel, B.; Rehr, J.; Conradson, S. Real-Space Multiple-Scattering Calculation and Interpretation of X-Ray-Absorption near-Edge Structure. *Phys. Rev. B: Condens. Matter Mater. Phys.* **1998**, *58*, 7565.
(25) Segall, M. D.; Lindan, P. J. D.; Probert, M. J.; Pickard, C. J.; Hasnip, P. J.; Clark, S. J.; Payne, M. C. *J. Phys.: Condens. Matter* **2002**, *14*, 2717−2744.
(26) Vanderbilt, D. *Phys. Rev. B: Condens. Matter Mater. Phys.* **1990**, *41*, 7892−7895.
(27) Perdew, J. P.; Burke, K.; Ernzerhof, M. *Phys. Rev. Lett.* **1996**, *77*, 3865−3868.
(28) Tkatchenko, A.; Scheffler, M. *Phys. Rev. Lett.* **2009**, *102*, 073005.
(29) Monkhorst, H. J.; Pack, J. D. *Phys. Rev. B* **1976**, *13*, 5188−5192.